npj Flexible Electronics

https://doi.org/10.1038/s41528-026-00568-y

Article in Press

# High-performance full-color afterglow organic light-emitting diodes with tri-mode emission and efficient energy transfer

Received: 23 December 2025

Accepted: 9 March 2026

Cite this article as: Cui, D., Xu, Z., Zhang, J. *et al.* High-performance full-color afterglow organic light-emitting diodes with tri-mode emission and efficient energy transfer. *npj Flex Electron* (2026). https://doi.org/10.1038/s41528-026-00568-y

**Dongyue Cui, Zhiwen Xu, Jingyu Zhang, Zhenli Guo, Peng Zhang, Chang Zeng, Shuhong Li, Yunlong Liu, Wenjun Wang, Hailin Qiu, Chao Zheng, Wei Huang & Runfeng Chen**

# High-performance Full-color Afterglow Organic Light-Emitting Diodes with Tri-mode Emission and Efficient Energy Transfer

Dongyue Cui[1], Zhiwen Xu[1], Jingyu Zhang[1], Zhenli Guo[1], Peng Zhang[1], Chang Zeng[1], Shuhong Li[3], Yunlong Liu[3], Wenjun Wang[3*], Hailin Qiu[4], Chao Zheng[1], Wei Huang[1, 2*], Runfeng Chen[1*]

[1]State Key Laboratory of Flexible Electronics (LoFE) & Institute of Advanced Materials (IAM), Nanjing University of Posts & Telecommunications, 9 Wenyuan Road, Nanjing 210023, China

[2]Institute of Flexible Electronics (IFE), Northwestern Polytechnical University, Xi'an 710072, Shaanxi, China

[3]Shandong Provincial Key Laboratory of Optical Communication Science and Technology, School of Physical Science and Information Technology, Liaocheng University, Shandong 252059, China

[4]Orient KOJI Limited, Tianjin 300122, P. R. China

**Authors:**

Dongyue Cui: c3096815938@163.com

Zhiwen Xu: 649660257@qq.com

Jingyu Zhang: sxxyzjy@126.com

Zhenli Guo: guozhenli96@163.com

Peng Zhang: zhangpeng7772023@163.com

Chang Zeng: 1028734438@qq.com

Shuhong Li: lishuhong@lcu.edu.cn

Yunlong Liu: liuyunlong@lcu.edu.cn

Hailin Qiu: qiuhailin@okinst.com

Chao Zheng: iamczheng@njupt.edu.cn

**Corresponding authors:**

Runfeng Chen: iamrfchen@njupt.edu.cn; 025-85866396

Wei Huang: iamwhuang@nwpu.edu.cn

Wenjun Wang: phywwang@163.com

**Keywords**: Afterglow OLEDs, Tri-mode afterglow, Full-color, Thick-layer architecture, Förster resonance energy transfer.

**Abstract**

Afterglow organic light-emitting diodes (OLEDs) with persistent emission after switching off the applied voltage have garnered extensive attention recently, but the available organic afterglow materials for electroexcitation remains rare, along with low device performance. Here, we report a series of high-performance full-color afterglow OLEDs by employing tri-mode afterglow molecule as emitting layer doped with various phosphorescent complexes in a simplified thick-layer OLED architecture. The tri-mode afterglow by transforming the long-lived ultralong phosphorescence to phosphorescence and fluorescence through thermally activated exciton release and reverse intersystem crossing promotes significantly the afterglow efficiency. Indeed, the tri-mode afterglow OLEDs display blue to cyan afterglow with lifetime up to 253 ms and maximum external quantum efficiency (EQE) of 7.4%. After doping of phosphorescent complexes, efficient energy transfer from the tri-mode afterglow host to phosphor dopants results in highly bright and efficient green, yellow and red afterglow OLEDs with the maximum lifetime of 132 ms, total EQE of 24%, and afterglow EQE of 3.6%, representing the highest efficiencies reported so far of afterglow OLEDs. This study opens exciting prospects for the development of high-performance afterglow OLEDs, leveraging unique properties of organic semiconductors with rich triplet excited state behaviors for advanced optoelectronic applications and light-emitting technologies.



**Introduction**

Organic light-emitting diodes (OLEDs) have become the highly promising technology for displays and lighting owing to their distinct merits of lightweight, flexibility, wide color range, and low power consumption[1, 2]. Recently, in addition to traditional prompt electroluminescence (EL), afterglow OLEDs that continue to emit light over 1 s (lifetime > 100 ms) after the applied voltage is turned off have attracted increasing attention[3-6] to take advantages of long-lived triplet excitons of room-temperature phosphorescent (RTP) or more precisely, organic ultralong RTP (OURTP) materials[7, 8] for a wide range of potential applications such as emergency and safety lighting, wearable and nighttime illumination, decorative or architecturally integrated displays and time-temperature indicators[9]. RTP and OURTP

materials relay on efficient intersystem crossing (ISC) promoted by hetero/heavy-atom incorporations[10, 11] and inter/intra-molecular interactions[12, 13] to facilitate exciton spin transformation from that on the lowest singlet excited state ($S_1$) to the lowest triplet excited state ($T_1$), while the spin-forbidden radiative decay of triplet exciton to the ground state ($S_0$) effectively elongates the lifetime of $T_1$ although generally with low RTP efficiency. Impressively, the unique purely organic RTP and OURTP materials with long-lasting photoluminescence (PL) have also shown great potential in advanced applications of information anti-counterfeiting[14], visual persistence displays[15], low-power indicators[16], and wearable optoelectronics[17]. However, to fabricate afterglow OLEDs, organic afterglow materials are essentially needed for the long-lasting EL after electroexcitation and more importantly, the emitting material should be semiconductive for electron and hole injection, transportation and recombination with matched fronter molecular orbital energy levels when used in the sandwich-structured devices[5, 6]. Therefore, the simultaneous requirement of afterglow feature and semiconductivity rules out a lot of organic luminescent materials, leading to rather rare applicable candidates for afterglow OLED emitters.

Adachi et al.[3] are the first to realize afterglow OLEDs using a deuterated RTP molecule as guest doped in a rigid steroid host modified by carbazole to increase the semiconductivity; the RTP afterglow OLED in normal phosphorescent OLED structure shows blue steady-state EL (SSEL) contributed mainly by the prompt fluorescence (PF) and green delayed EL from OURTP with lifetime up to 390 ms and total external quantum efficiency ($EQE_{total}$) around 1%. Following the RTP afterglow mechanism (Fig. 1a), our group[5] found that commercially available carrier transporting organic materials can be also used to construct afterglow OLEDs via host-guest doping; the resultant low-voltage driving (5.8 V) devices exhibit green OURTP with maximum $EQE_{total}$, luminance, and lifetime of 1.47%, 743 cd $m^{-2}$, and 356 ms, respectively. Su et al.[18] developed the thermally activated delayed fluorescence (TADF)-type afterglow OLEDs (Fig. 1b) using TADF molecule with moderate singlet-triplet spitting energy ($\Delta E_{ST}$ = 0.46 eV) and moderate reverse ISC (RISC) rate to slow down the delayed fluorescence (DF) for afterglow; the fabricated green TADF afterglow OLED with 10 wt% doped TADF emitter achieved an $EQE_{total}$ of 14.7% and an EL afterglow lifetime of 157 ms. We firstly reported the hybridized local and charge transfer-OURTP (HLCT-

OURTP) afterglow OLEDs (Fig. 1c) using a novel HLCT-OURTP molecule[6], which can turn the spin-forbidden triplet emission to the spin-allowed fluorescence through fast high-lying RISC process for high device efficiencies with the aid of its HLCT character, while its OURTP feature favors the long-lived afterglow lifetime of the EL emission when being doped in a rigid semiconductive host; a state-of-the-art maximum $EQE_{total}$ of 12% for the afterglow OLEDs was achieved along with an afterglow EQE ($EQE_{afterglow}$) of 3.11% reported for the first time. Adachi et al[4]. also realized the afterglow OLEDs based on exciplex organic long-persistent-luminescent (OLPL) systems (Fig. 1d) composed of a mixture of electron-donating and electron-accepting components, where charge separation, diffusion, and recombination will happen for the exciplex-type OLPL emission in the power-law decay behavior; an $EQE_{total}$ of ~0.7% and a green afterglow duration time of 17 s at a driving voltage of 40 V were observed. Recently, Xie et al.[9, 19] realized OLPL-type afterglow OLEDs (Fig. 1e) following the trap-induced persistent luminescence (TIP) mechanism by doping the TADF guest with low-lying the lowest unoccupied molecular orbital (LUMO) into a host to form trap state; under a driving voltage of 12 V, the device achieved an afterglow duration time up to 76 s and an $EQE_{total}$ of 2.31%. Despite these continued efforts in improving the afterglow OLEDs' efficiencies and lifetimes, the development of afterglow OLEDs remains at an infancy stage with significantly lower EQEs compared to these of conventional phosphorescent (37.3%)[20], TADF (43.3%)[21] and RTP (33.2%)[22] OLEDs, let alone the mainly green EL afterglow color.

To develop efficient afterglow OLEDs, we envision the previously reported tri-mode afterglow mechanism would be helpful[23, 24], by transforming the long-lived OURTP related to the radiative transition of the stabilized $T_1$ state ($T_1^*$) to $T_1$ emission for the delayed RTP (DRTP) through overcoming the exciton trapping depth ($\Delta E_{TD}$), followed by efficient RISC for the DF from the spin-allowed $S_1$ emission. With rationally modulated $\Delta E_{TD}$ and $\Delta E_{ST}$ to low values, the thermally activated exciton release (TAER) of $T_1^* \rightarrow T_1$ and RISC for $T_1 \rightarrow S_1$ will be significantly promoted and afterglow will be observed in OURTP, DRTP and DF (Fig. 1f), respectively. Similar to the RISC process in TADF molecules which is sensitive to $\Delta E_{ST}$, TAER process is sensitive to $\Delta E_{TD}$; when $\Delta E_{ST}$ and $\Delta E_{TD}$ are sufficiently low (< 0.37 eV)[25, 26],

thermal energy of the environment can overcome these energy gaps for the efficient RISC and TAER processes at room temperature. Indeed, when we employed a tri-mode afterglow emitter of 2,3,5,6-tetrakis(carbazol-9-yl)benzonitrile (4CzBN) as the emitting layer (EML) of OLEDs in a simplified thick-layer device architecture, blue to cyan EL afterglow with lifetimes from 197 to 253 ms was realized depending on the thickness of EML. Based on the cyan afterglow OLEDs, green, yellow, and red phosphorescent complexes were doped into the afterglow EML to achieve full-color afterglow OLEDs via energy transfer from the long-lived 4CzBN host to these colorful dopants (Fig. 1g).

Remarkably, the green, yellow and red afterglow devices exhibit corresponding afterglow lifetimes up to 132, 122 and 123 ms and the maximum $EQE_{total}$ of 24%, 22% and 24%, which are comparable with these of conventional phosphorescent OLEDs[27, 28] and represent the highest value of the reported afterglow OLEDs to date (Table S1). Notably, the $EQE_{afterglow}$ up to 3.6% figured out by a full-time-range lifetime measurement system was also the best result ever reported in afterglow OLEDs. Compared with the conventional multilayer structures of OLED devices, the simplified thick-layer architecture with fewer organic layers is beneficial, especially for the flexible electronics, to scalable device fabrication with reduced complexity and high device performance by reducing the refractive-index mismatch between organic layers[29, 30] and alleviating quenching of the long-lived triplet excitons[31, 32]. Therefore, this study significantly improves the performance of afterglow OLEDs by using the tri-mode afterglow emitter based on thick-layer OLED device architecture and efficient triplet excited state-involved energy transfer, representing significant concept breakthrough in modulating electronically pumped excited states for advanced flexible electronic applications.

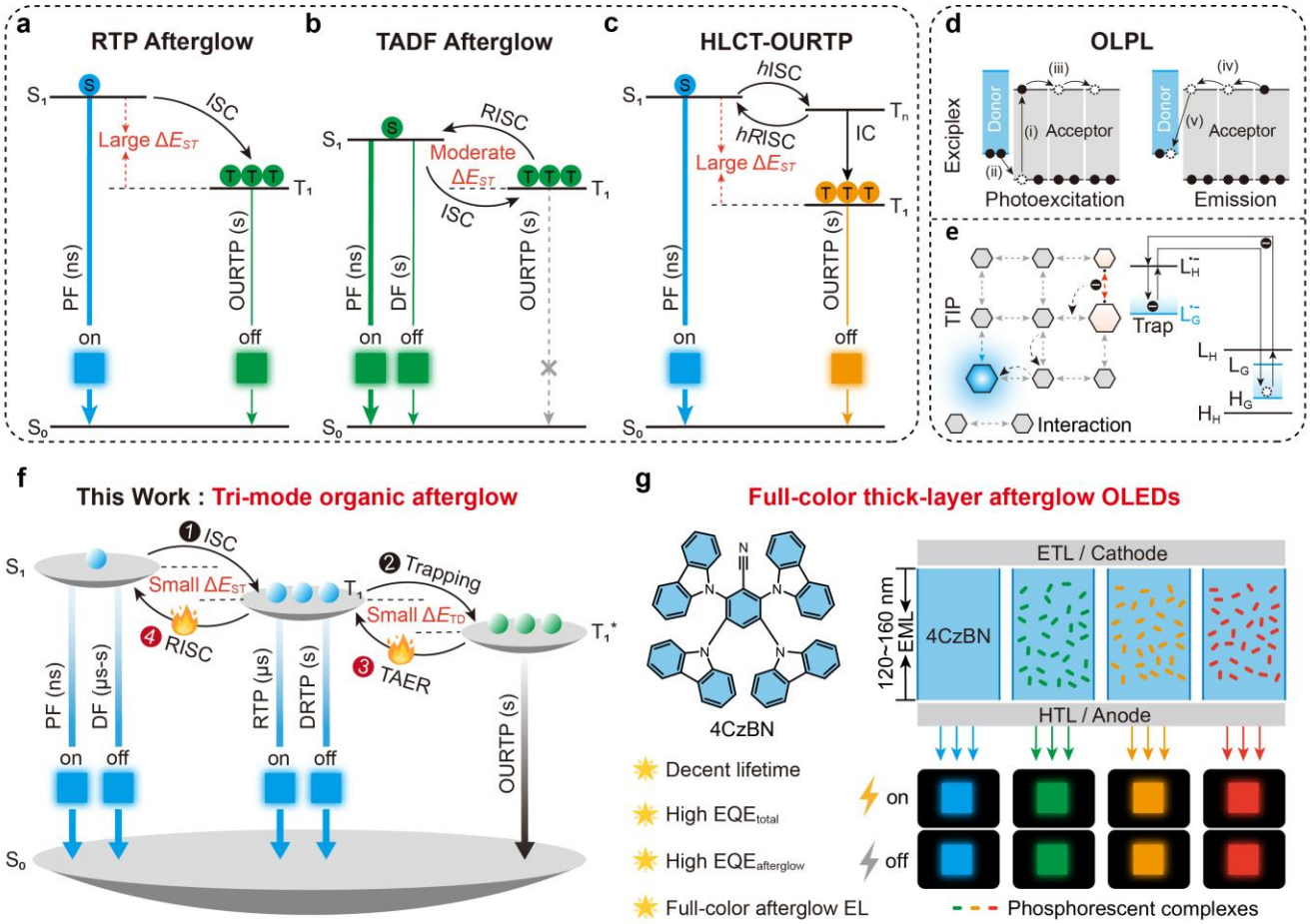


**Fig. 1** Organic afterglow mechanisms of **a** RTP afterglow, **b** TADF afterglow, (**c**) HLCT-OURTP, OLPL through **d** exciplex and **e** TIP emissions, and **f** tri-mode afterglow. **g** Tri-mode afterglow molecule of 4CzBN and the full-color thick-layer device structures with green, yellow and red phosphorescent metal dopants.

## Results

### Tri-mode afterglow behavior of 4CzBN.

The 4CzBN with four carbazole substituents on a central benzonitrile in donor-acceptor (D-A) structure was previously reported as a typical TADF molecule[33, 34], showing blue emissions with a small $\Delta E_{ST}$ of 0.19 eV in dilute 2-methyltetrahydrofuran (2-MeTHF) solution (Fig. 2a). Extraordinarily, we found that 4CzBN can exhibit a visible afterglow emission at room temperature when 4CzBN is in neat film or heavily doped in polymethyl methacrylate (PMMA) (Figs. S1-2). The steady-state PL (SSPL) spectrum (Fig. 2b) of the neat 4CzBN film is broad with a significantly red-shifted fluorescent peak at 460 nm (lifetime = 1.7 ns) (Fig. S3) compared to that in dilute solution (448 nm). And, the emission is stronger in

$N_2$ than in air, suggesting that the emission bands are related to triplet excited states that will be quenched by triplet $O_2$. From the delayed PL spectra with a delay time of 10 ms to eliminate the contribution of short-lived fluorescence, three distinct emission bands around 460, 494 and 538 nm appear with corresponding lifetimes of 232, 223 and 215 ms at room temperature (Fig. S4 and Table S2) and become more apparent at lower temperatures (Fig. 2c). Interestingly, the luminescent intensities of these three emission bands exhibit very different temperature-dependent behaviors: the 538 nm emission band show continual intensity enhancement as temperature drops; the 460 and 494 nm emission bands exhibit an initial slight intensity decrease when the temperature drops from 300 to ~240 K, and then enhance at further reduced temperatures, except for that the 460 nm emission intensity begins to decrease as temperature is lower than ~150 K (Fig. 2d). As to their lifetimes, different temperature-dependent behaviors were also observed, although they have similar lifetimes at room temperature. For the 460 and 494 nm emissions, the lifetimes elongate as temperature reduces from 300 to ~225 K and decrease rapidly when the temperature further drops to ~150 K followed by a slight lifetime increase at very low temperatures up to 78 K. For the 538 nm emission, the lifetime continuously elongates as temperature drops and reaches 1.2 s at 78 K (Fig. 2e). This spectacular temperature-dependent emission behaviors can be well explained by the previously reported tri-mode organic afterglow mechanism[23]. The three emission bands around 460, 494 and 538 nm are related to the radiative decay of $S_1$, $T_1$ and $T_1^*$ states for the DF, DRTP and OURTP, respectively. As the temperature reduces from 300 to 240 K, TAER is suppressed, leading to reduced intensities of the delayed emissions at 460 and 494 nm, while the also suppressed non-radiative transitions result in enhanced 538 nm emission and elongated lifetimes of the three emission bands. When the temperature further drops to ~150 K, both TAER and non-radiative transitions are significantly suppressed but the impact of TAER becomes lower, leading to significantly enhanced intensities of these three emission bands and the reduced lifetimes of the 460 and 494 nm emissions, because the lifetime inherited from $T_1^*$ through TAER is gradually blocked by low temperatures. At very low temperatures below 150 K, RISC also tends to be blocked, leading to the decreased intensity of DF

at 460 nm; the greatly suppressed non-radiative transitions resulting in increased lifetimes of all the three emission bands.

The experimental values of $\Delta E_{ST}$ and $\Delta E_{TD}$ for RISC and TAER processes are found to be 0.12 and 0.33 eV in 4CzBN neat film obtained from the onsets of the fluorescent, phosphorescent and OURTP spectra shown in Scheme S1. Such small values are highly favorable for the occurrence of the tri-mode afterglow and the larger $\Delta E_{TD}$ explains the more temperature sensitive TAER process than the RISC process. The tri-mode afterglow behavior of 4CzBN is also supported by the first principle theoretical calculations. Time-dependent density functional theory (TD-DFT) calculations reveal that 4CzBN possesses a very small $\Delta E_{ST}$ of 0.13 eV and singlet-triplet energy gaps of $S_1$-$T_1$/$T_2$ of 0.13 and 0.11 eV with corresponding large spin-orbit coupling (SOC) values of 0.11 and 0.66 $cm^{-1}$, which are characteristic features of typical TADF materials as reported previously[33, 34]. Notably, the SOC between $T_1$ and $S_0$ is as high as 5.04 $cm^{-1}$, which supports the possibility of efficient OURTP (Fig. 2f)[35]. In 4CzBN, the four donor units of carbazole are directly connected to the acceptor of benzonitrile in D-A structure, which typically results in a small $\Delta E_{ST}$ for facile RISC process[33, 34]. On the other hand, the abundant planar carbazole units are prone to forming H-aggregation[23, 24, 36], which can effectively stabilize $T_1$ to generate $T_1^*$ excitons. But, the twisted molecular structure of 4CzBN disrupts the π-π stacking[23] with distances from 3.4 to 3.6 Å between two intermolecular carbazoles as revealed by the molecular dynamics modelling[37] (Fig. S5), leading to a relatively smaller $\Delta E_{TD}$ to enable the efficient thermally activated TAER process at room temperature. It should be noted that the small $\Delta E_{TD}$ for the efficient TAER process is the key to realized the tri-mode afterglow; 1,2,3,5-tetrakis(carbazol-9-yl)-4,6-dicyanobenzene (4CzIPN), a classical TADF molecule structurally similar to 4CzBN, shows no afterglow in neat film because its large intermolecular π-π stacking distance (> 3.9 Å) prevents the formation of H-aggregation and the long-lived $T_1^*$ states (Fig. S6).

To determine the proportions of the long-lived emission of the tri-mode afterglow, the widely used spectrum deconvolution method was adopted[38]; by fitting the SSPL spectrum using the delayed PL spectrum and supposed fluorescent spectrum, the contribution of the long-lived (lifetime > 1 μs) emission

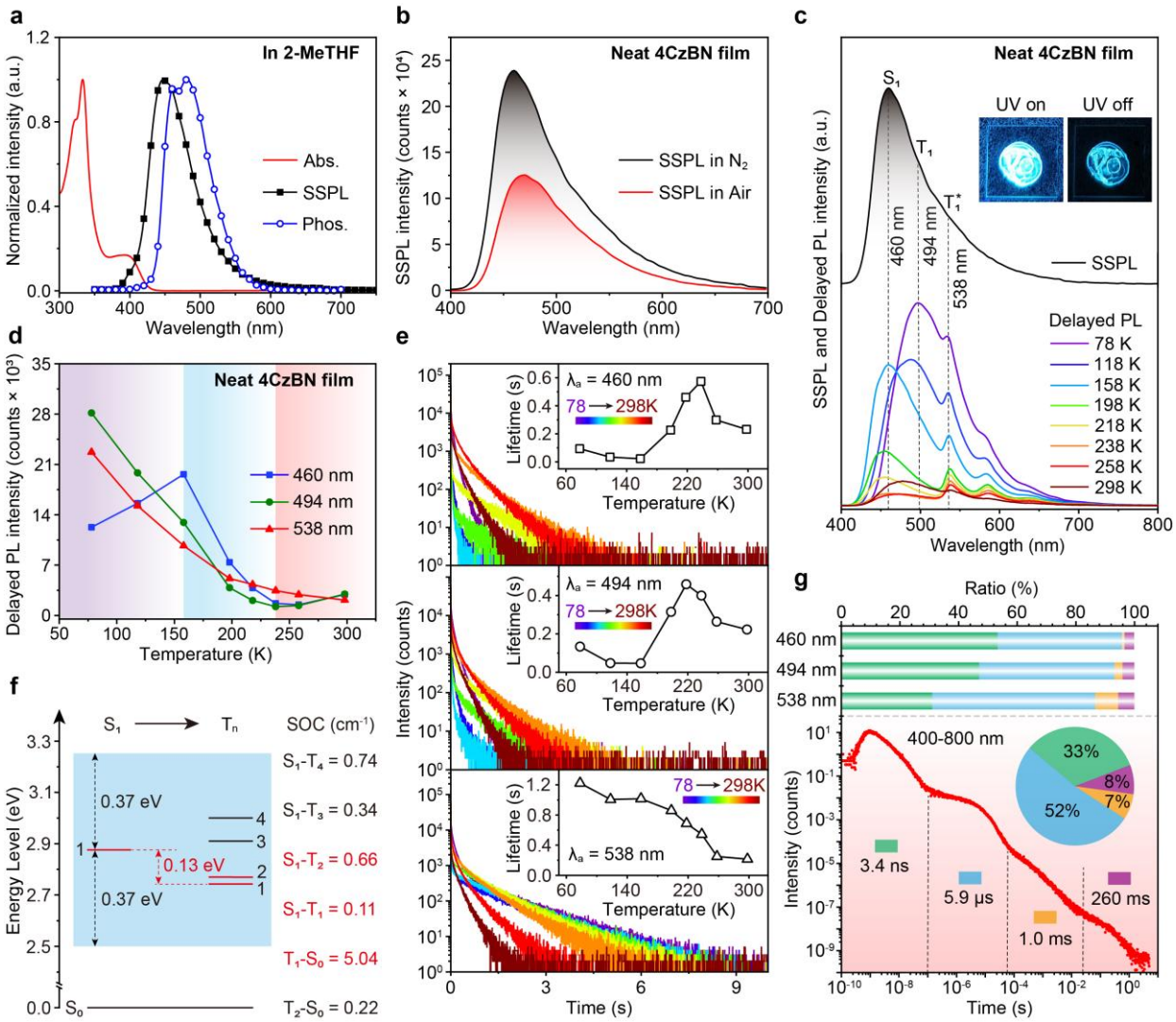


**Fig. 2 Tri-mode afterglow behavior of 4CzBN. a** Normalized absorption (Abs.) and SSPL spectra at room temperature and phosphorescence (Phos.) spectrum at 78 K in dilute 2-MeTHF. **b** SSPL spectra of 4CzBN neat film in $N_2$ and $O_2$ at room temperature. **c** SSPL spectrum at room temperature and temperature-dependent delayed PL spectra in film. **d** Temperature-dependent delayed PL intensity and **e** decay profiles of tri-mode afterglow peaks with lifetimes (inset) of the neat 4CzBN film. **f** TD-DFT calculated singlet and triplet excited state energies with corresponding SOC constants ($cm^{-1}$). **g** Full spectral range (400-800 nm) PL decay profile presented in a double-log form over a time range from ns to ms, along with the emission contributions at different time scales of the 460, 494, and 538 nm emissions. The spectra are all excited at 330 nm and the delay time is 10 ms.

is 58% (Fig. S7). Further, we used the full-time-range lifetime measurement technique to investigate the long-lived emission proportions[39]. It was found that owing to their rather broad and overlapped emission bands, three emission peaks at 460, 494, and 538 nm all have ns ($S_1 \rightarrow S_0$), μs ($T_1 \rightarrow S_1 \rightarrow S_0$ and $T_1 \rightarrow S_0$), and ms ($T_1^* \rightarrow T_1 \rightarrow S_1 \rightarrow S_0$, $T_1^* \rightarrow T_1 \rightarrow S_0$ and $T_1^* \rightarrow S_0$) scaled lifetimes (Figs. 2g and S8), and the μs and ms-scale emissions contribute as much as 67%, which is rather close to that by peak

deconvolution. Considering that only the ms-scaled emission meets the lifetime requirement of afterglow emission, the PL quantum yield (PLQY) of the afterglow of 4CzBN neat film was figured out to be around 7.7% from its contribution of 15% and the total PLQY of 51%.

**Non-doped tri-mode afterglow OLEDs.**

Inspired by the unique tri-mode afterglow behavior of 4CzBN in solid film and its previous applications in OLEDs,[33, 40] we applied it as EML in afterglow OLEDs to realize afterglow EL. It is worth noting that 4CzBN needs to be in aggregated states through heavy doping or in thick neat film to emit efficient afterglow emission (Figs. 2 and S9). And, the conventional device structures based on low doping contents and thin (~20 nm) EML are not suitable for preparing afterglow OLEDs (Fig. S10). Encouraged by the recently reported thick-layer OLEDs using thick EMLs[41-43], we fabricated tri-mode afterglow OLEDs with large thicknesses of 4CzBN EMLs of 120, 140 and 160 nm in a structure of indium tin oxide (ITO)/$MoO_3$ (3 nm)/mCP (15 nm)/4CzBN (120, 140, 160 nm)/TPBi (10 nm)/LiF (1 nm)/Al (100 nm), where 1,3-di(9*H*-carbazol-9-yl)benzene (mCP) and 2,2',2''-(1,3,5-benzenetriyl)-tris(1-phenyl-1*H*-benzimidazole) (TPBi) serve as the hole- and electron-transporting layers, respectively (Figs. 3a and S11). Notably, the thick OLEDs with broad exciton recombination zone and reduced exciton quenching caused by interfaces and electrodes[44, 45] would favor the efficient long-lived electrically driven afterglow, especially because the HOMO and LUMO levels of 4CzBN are well aligned with the energy level requirements of the thick device for good charge carrier balance[41-43].

Excitingly, the rationally designed devices can be turned on at a low driving voltage of 3.2 V, showing maximum luminance and maximum current density up to 13160 cd $m^{-2}$ and 608 mA $cm^{-2}$, respectively (Fig. 3b). From their different device performance in terms of power efficiency (PE), current efficiency (CE), $EQE_{total}$ and $EQE_{afterglow}$ ranging from 5.4, 14 to 10 lm $W^{-1}$, 6.3, 15 to 11 cd $A^{-1}$, 3.1, 7.4 to 5.8%, and 0.47, 1.10 to 0.87%, the optimal thickness of 4CzBN EML is 140 nm for the highest device efficiencies (Figs. 3c and S12). The SSEL and delayed EL spectra are almost identical to PL spectra, showing a red-shifted and broader afterglow EL after a delay time of 10 ms to eliminate the

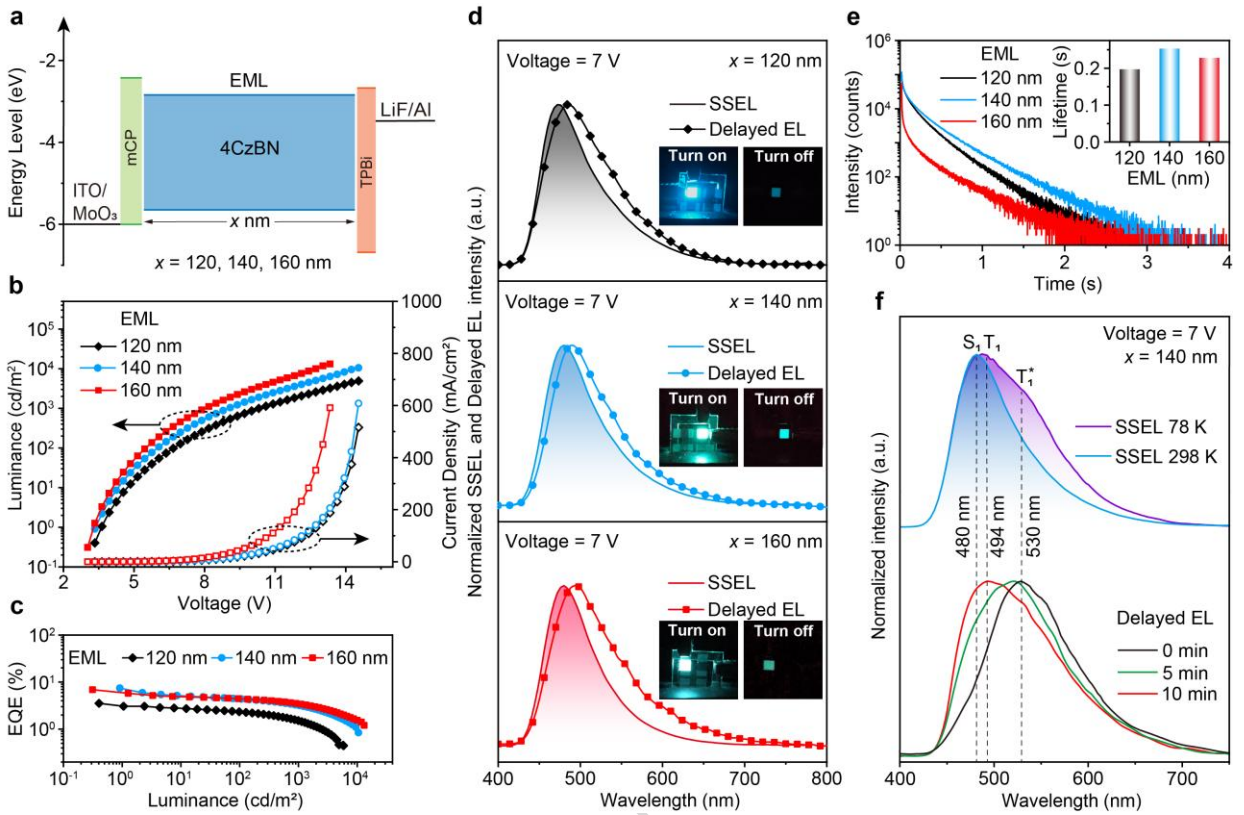


**Fig. 3 Non-doped thick-layer afterglow OLEDs. a** Device structure, **b** luminance-current density-voltage **c** and $EQE_{total}$ -luminance curves, **d** SSEL and delayed EL (delay 10 ms) spectra with corresponding photographs (inset) when the applied voltage (7 V) is turned on or off, **e** EL decay profiles (484, 490 and 494 nm) and lifetimes (inset) at different thickness of EML. **f** SSEL spectra of the 140 nm-thick-device at 78 and 298 K and the delayed EL spectra at low temperatures when being warmed from 78 K for 5 and 10 min in a room-temperature atmosphere.



contributions of short-lived prompt fluorescence (Fig. 3d and Movie S1). Notably, there is an 8 nm redshift when the EML thickness increases from 120 to 160 nm, possibly due to the microcavity effects of the devices[46, 47]. And, the EML thickness dependent behavior was also observed in the afterglow EL decay, showing different lifetimes of 197, 253 and 228 ms for the devices with EML thickness of 120, 140 and 160 nm, respectively (Fig. 3e). In contrast, the contributions of RTP, DRTP and OURTP emissions to the SSEL and delayed EL keep nearly constant at different EML thicknesses (Fig. S13). Therefore, the different lifetimes might be related to also the varied microcavity effects and/or the different recombination zones of the devices[48, 49].

When the EL spectra were measured at low temperatures, the SSEL of the 140 nm thick device also becomes broader due to the contributions of markedly enhanced long-lived emission of $T_1$ and $T_1^*$, as

evidenced by the significantly red-shifted delayed EL spectra (Fig. 3f). When the temperature is gradually increased from 78 K for 5 and 10 min, the OURTP-dominated delayed EL spectra blue shift gradually, revealing that the TAER and RISC processes are gradually activated to trigger the DRTP and DF emissions from $T_1$ and $S_1$. Moreover, the non-doped afterglow device exhibited no significant shortening or aging of the afterglow EL lifetime under repeated voltage on/off switching at a driving voltage of 7 V, indicating good operational stability (Fig. S14).

**Mechanism of the tri-mode afterglow OLEDs.**

Based on the tri-mode afterglow behavior of 4CzBN upon photoexcitation, the mechanism of electro-excited tri-mode afterglow of the non-doped OLEDs can be proposed. When the voltage is turned on, holes and electrons are injected, transported and finally recombined on EML of 4CzBN to form excitons. Approximately 25% excitons populate the $S_1$ state, generating prompt fluorescence emission, while the remaining 75% excitons occupy the $T_1$ and $T_1^*$ states to exhibit long-lived RTP and OURTP emissions. The long-lived excitons on $T_1^*$ can transfer to $T_1$ and $S_1$ states through the TAER and RISC processes with the aid of thermal energy, resulting in DRTP and DF emissions. After the voltage is turned off, the prompt emissions disappear immediately. The remaining long-lived triplet excitons generate the tri-mode afterglow EL through direct emission of $T_1^*$ for OURTP, the TAER to populate $T_1$ for DRTP, and TAER and RISC processes to populate $S_1$ for DF (Fig. 4a). Notably, the realization of blue to cyan afterglow OLEDs lays the foundation for extending afterglow devices across the full visible spectrum by energy transfer from the bluish afterglow of 4CzBN to various emitters[50, 51]. In this sense, we rationally selected three phosphorescent Ir(III) complexes of bis[2-(2-pyridinyl-N)phenyl-C](acetylacetonato) iridium(III) ($Ir(ppy)_2acac$), bis(2-phenylbenzothiazolato) (acetylacetonate) iridium(III)($Ir(bt)_2acac$) and bis(1-phenylisoquinoline) (acetylacetonate)iridium(III) ($Ir(piq)_2acac$), which show green, yellow and red emissions, respectively. These phosphorescent emitters exhibit significant spectral overlap between their absorption spectra (in dilute solution) and the SSPL and delayed PL spectra of neat 4CzBN film, ensuring the efficient energy transfer (Fig. S15).

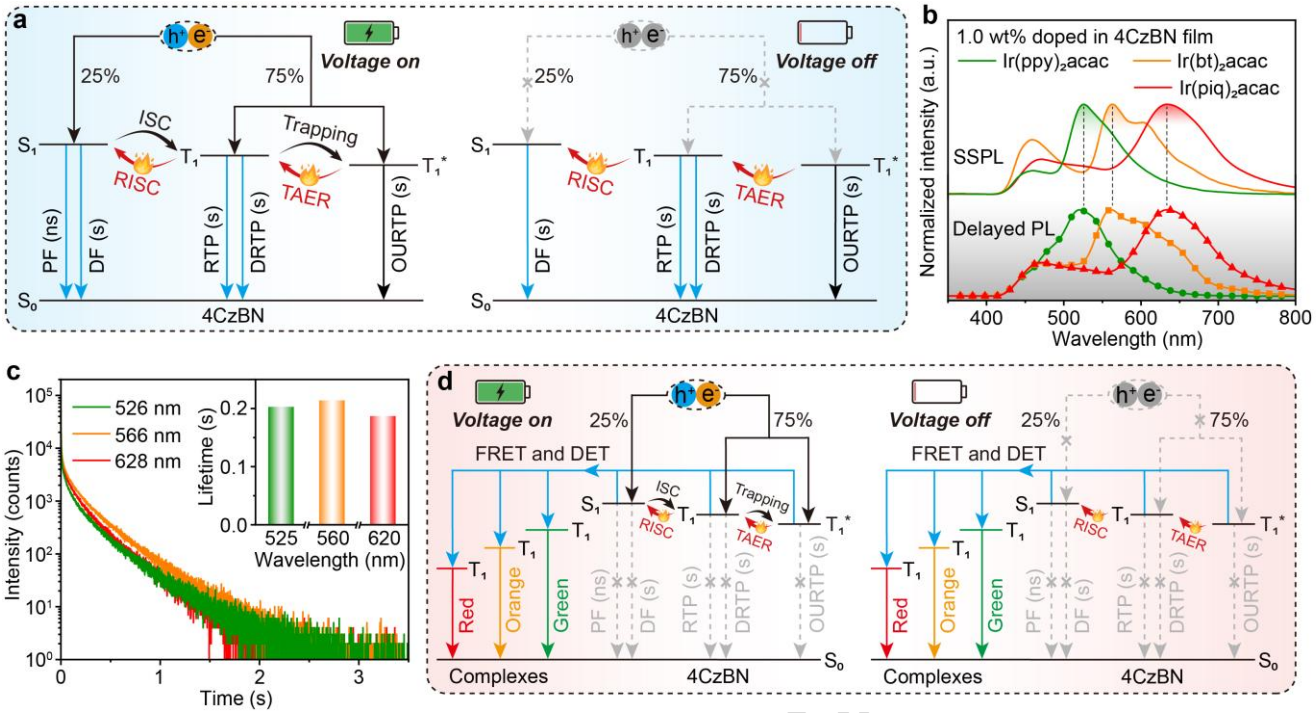


**Fig. 4 a** Mechanisms of tri-mode afterglow EL based on thick EML of 4CzBN. **b** SSPL and delayed PL (delay 10 ms) spectra and **c** decay profiles and lifetimes (inset) of 526, 566 and 628 nm emission after doping 1.0 wt% $Ir(ppy)_2acac$, $Ir(bt)_2acac$ and $Ir(piq)_2acac$ in 4CzBN film upon 330 nm excitation. **d** Mechanisms to realize full-color afterglow EL.

Indeed, the SSPL of the doped films prepared by doping the three phosphorescent emitters into 4CzBN at a content of 1.0 wt% show two emission peaks upon photoexcitation. The short-wavelength emission peak around 467 nm originates from 4CzBN, while the long-wavelength emission peaks at 526 nm, 566 nm and 628 nm are corresponding to the emissions from these phosphorescent emitters (Figs. 4b and S16). To our delight, all three doped films exhibit prominent afterglow emissions, showing dual emission peaks corresponding to both 4CzBN and the phosphorescent emitters (Fig. 4b). The photo-excited emission lifetimes at 526, 566, and 628 nm for green, yellow and red afterglow are 204, 214, and 187 ms (Fig. 4c), respectively. The shorter lifetimes of these emissions than the pristine blue afterglow of 4CzBN host along with the reduced lifetime of 4CzBN emission (467 nm) upon the increased doping contents of phosphorescent emitters (Fig. S17) indicate the efficient long-lived triplet excited state-related energy transfer via Förster resonance energy transfer (FRET) and Dexter energy transfer (DET) from 4CzBN to these phosphorescent complex dopants[50, 51]. Encouraged by the successfully realized full-color afterglow of the

host-guest system upon photoexcitation, we can expect the realization of efficient full-color afterglow EL, since triplet excitons can be directly generated upon electroexcitation in a ratio of 75% (Fig. 4d).

**Full-color afterglow OLEDs.**

The devices were constructed in an identical structure of the non-doped thick-layer afterglow OLEDs, where the EMLs with the optimal thickness of 140 nm were co-deposited using the phosphorescent complexes and 4CzBN. The dopants of $Ir(ppy)_2acac$, $Ir(bt)_2acac$ and $Ir(piq)_2acac$ were doped into 4CzBN at different contents of 0.5, 1.0, and 5.0 wt% for green (Device G), yellow (Device Y) and red (Device R) devices, respectively (Fig. S18). The devices performance was optimized and the optimal doping contents of the phosphorescent complexes is 1.0 wt% $Ir(ppy)_2acac$, 1.0 wt% $Ir(bt)_2acac$, and 0.5 wt% $Ir(piq)_2acac$, respectively (Fig. 5a). At such low doping levels, the direct trapping of charge carriers on the metal complexes would be significantly low[52, 53]. And, distinct green, yellow and red afterglow EL emissions were successfully observed. Unlike photoexcitation, SSEL spectra have no emission bands of 4CzBN at even lower doping content, suggesting the enhanced energy transfer under the local electric fields[54] and with better spectral overlap by the facilitated TAER and RISC processes for DRTP and DF to blue shift the emission spectrum at increased temperature when the device is on operation. The combined effects of the electric and thermal fields in OLEDs should be responsible for the much higher energy transfer efficiency under electroexcitation. The delayed EL spectra are closely matched with the SSEL spectra, indicating that all emissions are originated from the doped emitters and the energy transfer from the long-lived 4CzBN to the dopants is efficient and complete (Fig. 5b).

Impressively, the EL lifetimes of the green, yellow and red OLEDs are extraordinary long, reaching up to 132, 122 and 123 ms at an applied voltage of 7 V (Fig. 5c). The shorter lifetimes of the green, yellow and red afterglow OLEDs than that of the dopant-free blue afterglow OLED (lifetime = 253 ms) (Fig. S19) suggest again the efficient energy transfer from the long-lived 4CzBN to the colorful dopants. Considering that triplet excitons have very long lifetime and diffusion length, both the long-ranged (up to 10 nm) FRET and short-ranged (< 1 nm) DET from the energy donor of 4CzBN to the closely contacted phosphorescent dopants at low doping levels should play important roles here[55, 56]. The turn-on voltages,

maximum luminance and current-density of the doped afterglow OLEDs are 5.2, 3.9 and 4.5 V; 65781, 47274 and 22873 cd $m^{-2}$; and 369, 353 and 550 mA $cm^{-2}$ (Fig. 5d), respectively. Extraordinary, the green, yellow, and red afterglow OLEDs exhibited high CE, PE and $EQE_{total}$ of 44, 55 and 13 lm $W^{-1}$; 72, 55 and 20 cd $A^{-1}$; 24%, 22% and 24%, respectively (Fig. 5e); these values represent the highest performance reported to date among all afterglow OLEDs (Tables S1 and S3). Moreover, the $EQE_{afterglow}$ of these high-performance afterglow devices would be as high as 3.6%, 3.3% and 3.6%, assuming that the proportion of long-lived emission is 15% revealed by photophysical investigations (Fig. 2g) and the energy transfer from 4CzBN to dopants is completely. Notably, these results break the records of $EQE_{afterglow}$ of afterglow OLEDs up to date, since the long-lived spin-forbidden triplet excitons can be successfully transformed to $S_1$ for the spin-allowed DF through TAER and RISC and to the excited states of metal-complex for efficient phosphorescence through energy transfer. It should be noted thus obtained $EQE_{afterglow}$ may differ from the actual situation, because photonic and electrical excitations have different mechanisms in exciton formation pathways and energy transfer dynamics. Upon electroexcitation, 75% excitons are triplet without need of ISC, which may breakthrough the long-lived emission proportion of 15% observed photo physically and the DET process will be more favorable; also, the electric field can directly influence the electron cloud overlap and energy barrier between the donor and acceptor for the enhanced energy transfer[54]. Moreover, elevated temperature on the operation of OLEDs will facilitate the TAER and RISC processes for the enhanced delayed emissions and energy transfer. Principally, directly measuring the contribution of afterglow emission to the total electroluminescence under electrical excitation would be the most accurate way to determine $EQE_{afterglow}$. However, due to current technical limitations and huge difficulties to measure the afterglow photon flux relative to the steady-state flux upon electronic excitation, applicable methods to measure $EQE_{afterglow}$ directly are yet to be developed, along with rarely reported $EQE_{afterglow}$ values of afterglow OLEDs[6].

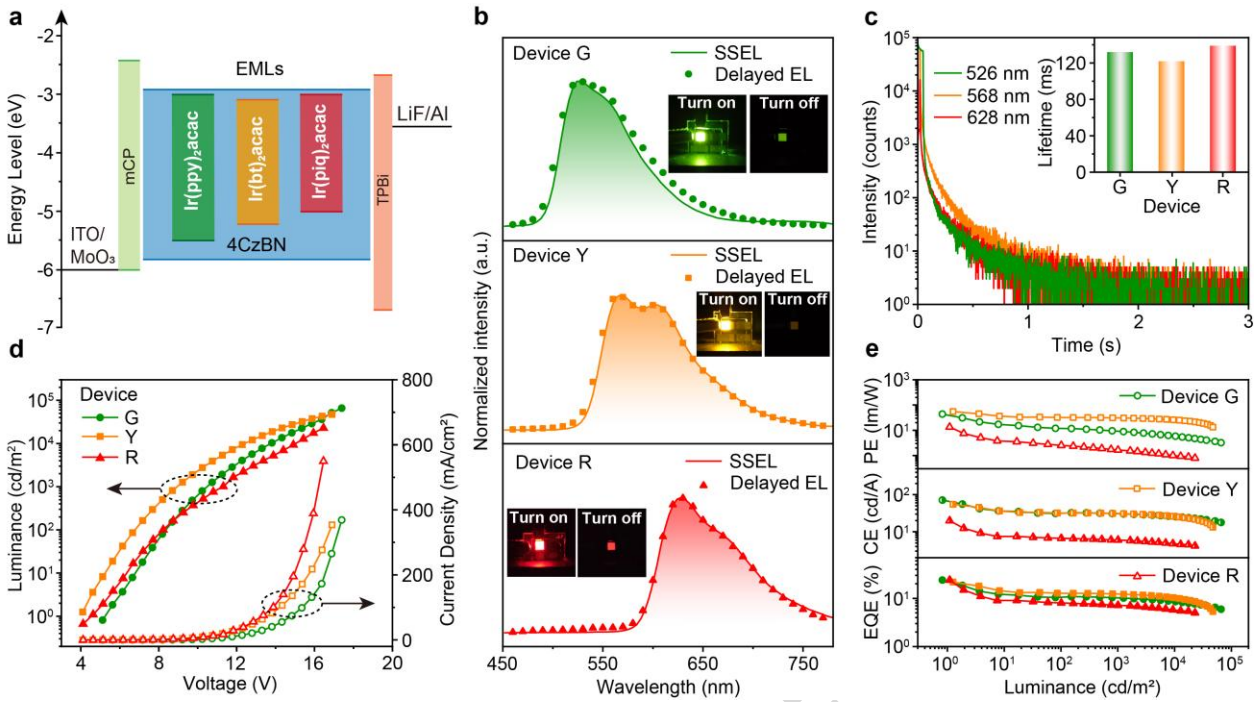


**Fig. 5** High-performance green, yellow and red afterglow OLEDs. **a** Device structure, **b** SSEL and delayed EL (delay 10 ms) spectra with corresponding photographs (inset) when the applied voltage (7 V) is turned on or off, **c** EL decay profiles and lifetimes (inset) measured using a driving voltage of 7 V, **d** luminance-current density-voltage and **e** efficiency-luminance curves.

## Discussion

In summary, we report for the first time that the conventional TADF molecule of 4CzBN exhibits the unique tri-mode afterglow at the aggregated state, featuring an afterglow PLQY of 7.7% and a lifetime of ~230 ms at room temperature. Based on this extraordinary excitonic behavior, we designed and fabricated high-performance blue to cyan afterglow OLEDs in a simplified thick-layer architecture with different thicknesses of 4CzBN EML up to 160 nm; the non-doped devices deliver excellent afterglow EL performance, exhibiting a maximum $EQE_{total}$ of 7.4% and $EQE_{afterglow}$ of 1.10%, and an afterglow EL lifetime over 250 ms. Furthermore, through efficient energy transfer from the cyan afterglow to green, yellow, and red dopants, full-color afterglow OLEDs were realized, where the dopant molecules effectively harvest excitonic energy and inherit lifetime of the long-lived 4CzBN excitons in tri-mode afterglow observed firstly in electroluminescence. The colorful devices exhibit record-high $EQE_{total}$ values of 24%, 22%, and 24% for green, yellow and red OLEDs, representing the highest efficiencies reported to date for afterglow OLEDs. Also, a maximum $EQE_{afterglow}$ of 3.6% was identified, breaking

through the efficiency limit of afterglow OLEDs. These advances, based on the novel tri-mode afterglow mechanism in designing high-performance color-tunable organic afterglow OLEDs, hold promising potential for a wide array of optoelectronic applications, including advanced display technologies, information encryption, visual sensing, and next-generation lighting techniques.

## Methods

### Materials and characterization

The materials used in this research include 2,3,5,6-tetrakis(carbazol-9-yl)benzonitrile (4CzBN) from Suzhou GeAo New Materials Co., Ltd.; 2,2',2''-(1,3,5-benzinetriyl)-tris(1-phenyl-1H-benzimidazole) (TPBi), 1,2,3,5-tetrakis(carbazol-9-yl)-4,6-dicyanobenzene (4CzIPN), bis[2-(2-pyridinyl-N)phenyl-C](acetylacetonato)iridium(III) (Ir(ppy)2acac), bis(2-phenylbenzothiazolato)(acetylacetonate)iridium(III) (Ir(bt)2acac) and bis(1-phenylisoquinoline)(acetylacetonate)iridium(III) (Ir(piq)2acac) from Xi'an Yuri Solar Co., Ltd.; and 1,3-di(9H-carbazol-9-yl)benzene, also known as N,N′-dicarbazolyl-3,5-benzene (mCP), from Jilin OLED Material Tech Co., Ltd. Poly(methyl 2-methylpropenoate) (PMMA) with a weight-average molecular weight of approximately 150000, and the organic solvents of 2-methyl-tetrahydrofuran (2-MeTHF) and dichloromethane (DCM) were purchased from Energy Chemical. All the organic materials and solvents were used directly without further purification. Ultraviolet-visible (UV-Vis) absorption spectra in solution were tested on a Jasco V-750 spectrophotometer under ambient conditions. Steady-state photoluminescent (SSPL) and delayed photoluminescent (PL) spectra (delay time of 10 ms), steady-state electroluminescence (SSEL) and delayed electroluminescence (EL) spectra, as well as PL and EL decays were measured on an Edinburgh FLS 980 fluorescence spectrophotometer equipped with a xenon arc lamp (Xe 900), a microsecond flash-lamp (μF 900), Function Generator (AFG3021C) and some picosecond pulsed light emitting diodes (LEDs) with several wavelengths. The PL and EL decay measurements were performed using two complementary detection modes: (1) the Time-Correlated Single Photon Counting (TCSPC) technique with the Time-Correlated Counter 900 (TCC900) acquisition

card, and a picosecond-pulsed LED as the excitation source for lifetimes in the range of approximately 100 ps to 10 μs, and (2) the Multi-Channel Scaling (MCS) mode with the Photon Counting Scaler 900 (PCS900) fast counter card and μF 900 or AFG3021C as the excitation source for longer lifetimes from about 1 μs to 10 s. The emission signal was collected by a photomultiplier tube (PMT) synchronized with the excitation pulse.

**Device fabrication and characterization**

In a general procedure, the indium tin oxide (ITO) substrates were washed by deionized water, acetone, and ethanol for 30 min in an ultrasonic bath and then treated with ultraviolet (UV)-ozone for 15 min. Devices were fabricated by evaporating organic layers at a rate of 0.05-0.2 nm $s^{-1}$ at a pressure below $5\times10^{-4}$ Pa. Onto the electron-transporting layer, a layer of LiF with a 1 nm thickness was deposited at a rate of 0.01 nm $s^{-1}$. Finally, a 100-nm-thick layer of Al was deposited at a rate of 0.5 nm $s^{-1}$ as the cathode. All non-doped tri-mode afterglow OLEDs possess a structure of indium tin oxide (ITO)/MoO3 (3 nm)/mCP (15 nm)/4CzBN (20, 80, 100, 120, 140 and 160 nm)/TPBi (10 nm)/LiF (1 nm)/Al (100 nm), while the colorful afterglow OLEDs are fabricated by doping the metal complexes into the 4CzBN host with the EML thickness of 140 nm. All the devices were characterized immediately at room temperature after encapsulation. The luminance-voltage-current density, CE and PE curves were recorded using a Keithley 2400 voltage current source and a calibrated luminance meter, respectively. EL spectra were measured by a spectra-scan PR655 spectrophotometer. The delayed EL spectra and lifetimes were measured using Edinburgh FLS980 fluorescence spectrophotometer with a 10 ms delay time by a short pulse (frequency: 20 Hz; pulse width: 20 ms).



**Acknowledgements**

This study was supported by the National Natural Science Foundation of China (No. 22275097 focused on organic afterglow materials and afterglow OLEDs, No. 62374093 focused on host-guest organic after-

glow materials and No. 62288102 focused on flexible electronic materials and devices), State Key Laboratory of Advanced Optical Communication Systems and Networks Shanghai Jiao Tong University (No. 2024GZKF001 focused on organic afterglow luminescent mechanism and applications), Open Fund of the State Key Laboratory of Luminescent Materials and Devices (No. 2024-skllmd-10 focused on organic afterglow materials and applications), and the Postgraduate Research & Practice Innovation Program of Jiangsu Province (No. KYCX221000 and No. KYCX220250 focused on RTP OLEDs and host-guest luminescent materials, respectively). We thank the Orient KOJI Limited for providing technical support for full-time-range lifetime measurements.



**Author details**

[1]State Key Laboratory of Flexible Electronics (LoFE) & Institute of Advanced Materials (IAM), Nanjing University of Posts & Telecommunications, 9 Wenyuan Road, Nanjing 210023, China. [2]Institute of Flexible Electronics (IFE), Northwestern Polytechnical University, Xi'an 710072, Shaanxi, China. [3]Shandong Provincial Key Laboratory of Optical Communication Science and Technology, School of Physical Science and Information Technology, Liaocheng University, Shandong 252059, China. [4]Orient KOJI Limited, Tianjin 300122, P. R. China.

**Author Contributions**

D.Y.C. and R.F.C. conceived the experiments. D.Y.C., R.F.C., W.J.W., and W.H. wrote the manuscript. D.Y.C. prepared the samples and OLED devices, and conducted the analysis and characterization of photophysical properties and device performance. Z.W.X., J.Y.Z., Z.L.G., S.H.L., and Y.L.L. discussed the results and provided the suggestions for the manuscript. C.Z. (Chao Zheng) provided suggestions on sample preparation and characterization. P.Z. and C.Z. (Chang Zeng) were responsible for theoretical calculations of excited-state energies and molecular dynamics modelling, respectively. H.L.Q. used the full-time-range lifetime measurement technique to investigate the long-lived emission proportions. All authors contributed to the discussion of the results.

**Data availability**

All data are available in the manuscript or the supplementary information.

**Conflict of interest**

Author Wei Huang is Editor-in-Chief of npj Flexible Electronics. Wei Huang was not involved in the journal's review of, or decisions related to, this manuscript. The authors declare no competing financial interests and no patents have been applicated.

**References**


1. Diesing, S., Zhang, L., Zysman-Colman, E. & Samuel, I. D. W. A figure of merit for efficiency roll-off in TADF-based organic LEDs. *Nature* **627,** 747-753 (2024).
2. Pashaei, B. et al. Polypyridyl ligands as a versatile platform for solid-state light-emitting devices. *Chem. Soc. Rev.* **48,** 5033-5139 (2019).
3. Kabe, R., Notsuka, N., Yoshida, K. & Adachi, C. Afterglow Organic Light-Emitting Diode. *Adv. Mater.* **28,** 655-660 (2016).
4. Tan, S., Jinnai, K., Kabe, R. & Adachi, C. Long-Persistent Luminescence from an Exciplex-Based Organic Light-Emitting Diode. *Adv. Mater.* **33,** 2008844 (2021).
5. Xie, G. Z. et al. Achieving low driving voltage and highefficiency afterglow organic light-emitting diodes through host-guest doping. *Appl. Phys. Rev.* **9,** 031410 (2022).
6. Cui, D. Y. et al. Hybrid Local and Charge-Transfer Material with Ultralong Room Temperature Phosphorescence for Efficient Organic Afterglow Light-Emitting Diodes. *Angew. Chem., Int. Ed.* **63,** e202411588 (2024).
7. Xie, G. Z. et al. Resonance-Induced Dynamic Triplet Exciton Population for Photoactivated Organic Ultralong Room Temperature Phosphorescence. *J. Am. Chem. Soc.* **146,** 20449-20457 (2024).
8. Yu, Q. C. et al. Ligand-to-Ligand Charge Transfer Induced Red-Shifted Room Temperature Phosphorescence in Metal-Organic Frameworks. *J. Am. Chem. Soc.* **147,** 10530-10539 (2025).
9. Wu, Z. S. et al. Trap-induced persistent luminescence in organic light-emitting diodes. *InfoMat* **7,** e12657 (2025).
10. Guo, W. J. et al. Isomeric Engineering of Organic Luminophores for Multicolor Room Temperature Phosphorescence Including Red Afterglow. *Adv. Funct. Mater.* **34,** 2406888 (2024).
11. Peng, Y. Q. et al. Multilevel Stimulus-Responsive Room Temperature Phosphorescence Achieved by Efficient Energy Transfer from Triplet Excitons to Mn2+ Pairs in 2D Hybrid Metal Halide. *Adv. Funct. Mater.* **35,** 2420311 (2025).

12. Li, H. et al. Fluorine-induced aggregate-interlocking for color-tunable organic afterglow with a simultaneously improved efficiency and lifetime. *Chem. Sci.* **12,** 3580-3586 (2021).
13. Zhou, L. et al. High-efficiency color-tunable ultralong room-temperature phosphorescence from organic-inorganic metal halides via synergistic inter/intramolecular interactions. *Chem. Sci.* **15,** 10046-10055 (2024).
14. Gong, Y. Q. et al. Spectral and Temporal Manipulation of Ultralong Phosphorescence Based on Melt-Quenched Glassy Metal-Organic Complexes for Multi-Mode Photonic Functions. *Adv. Funct. Mater.* **34,** 2312491 (2024).
15. Li, X. et al. Bright and Ultralong Organic Phosphorescence via Sulfonic Acid Functionalization for High-Contrast Real-Time Light-Writing Display. *J. Am. Chem. Soc.* **147,** 14198-14210 (2025).
16. Liang, Y. C. et al. Thermally Enhanced Phosphorescent Carbon Nanodots for Monitoring Cold-Chain Logistics. *Small.* **20,** 2312218 (2024).
17. Gan, N. et al. Stretchable phosphorescent polymers by multiphase engineering. *Nat. Commun.* **15,** 4113 (2024).
18. Qiu, W. D. et al. Afterglow OLEDs incorporating bright closely stacked molecular dimers with ultra-long thermally activated delayed fluorescence. *Matter* **6,** 1231-1248 (2023).
19. Lin, C. J. et al. Charge trapping for controllable persistent luminescence in organics. *Nat. Photon.* **18,** 350-356 (2024).
20. Cao, L. Y., Zhu, Z. Q., Klimes, K. & Li, J. Efficient and Stable Molecular-Aggregate-Based Organic Light-Emitting Diodes with Judicious Ligand Design. *Adv. Mater.* **33,** 2101423 (2021).
21. Ge, L. S. et al. Efficient and Stable Narrowband Pure-Red Light-Emitting Diodes with Electroluminescence Efficiencies Exceeding 43%. *J. Am. Chem. Soc.* **146,** 32826-32836 (2024).
22. Zeng, J. J. et al. Purely organic room-temperature phosphorescence sensitizers for highly efficient hyperfluorescence OLEDs. *Sci. Adv.* **11,** eadt7899 (2025).
23. Jin, J. B. et al. Thermally activated triplet exciton release for highly efficient tri-mode organic afterglow. *Nat. Commun.* **11,** 842 (2020).

24. Jin, J. J. et al. Modulating Tri-Mode Emission for Single-Component White Organic Afterglow. *Angew. Chem., Int. Ed.* **60,** 24984-24990 (2021).

25. Yang, Z. et al. Recent advances in organic thermally activated delayed fluorescence materials. *Chem. Soc. Rev.* **46,** 915-1016 (2017).

26. Zheng, X. et al. Achieving 21% External Quantum Efficiency for Nondoped Solution-Processed Sky-Blue Thermally Activated Delayed Fluorescence OLEDs by Means of Multi-(Donor/Acceptor) Emitter with Through-Space/-Bond Charge Transfer. *Adv. Sci.* **7,** 1902087 (2020).

27. Gnanasekaran, P. et al. Perceiving the influence of phenyl-carbazole isomers on sulfone/thioxanthone-based D-A-D hosts: realizing efficient red-phosphorescent OLEDs. *J. Mater. Chem. C.* **12,** 2203-2215 (2024).

28. Kim, H. G., Kim, K. H. & Kim, J. J. Highly Efficient, Conventional, Fluorescent Organic Light-Emitting Diodes with Extended Lifetime. *Adv. Mater.* **29,** 1702159 (2017).

29. Li, Y. et al. Optical Outcoupling Efficiency of Organic Light-Emitting Diodes with a Broad Recombination Profile. *Adv. Opt. Mater.* **9,** 2001812 (2021).

30. Xu, R.-P., Li, Y.-Q. & Tang, J.-X. Recent advances in flexible organic light-emitting diodes. *J. Mater. Chem. C.* **4,** 9116-9142 (2016).

31. Sachnik, O. et al. Single-Layer Organic Light-Emitting Diode with Trap-Free Host Beats Power Efficiency and Lifetime of Multilayer Devices. *Adv. Mater.* **36,** 2311892 (2024).

32. Zhao, H., Arneson, C. E., Fan, D. & Forrest, S. R. Stable blue phosphorescent organic LEDs that use polariton-enhanced Purcell effects. *Nature* **626,** 300-305 (2024).

33. Zhang, D. D. et al. Sterically shielded blue thermally activated delayed fluorescence emitters with improved efficiency and stability. *Mater. Horiz.* **3,** 145-151 (2016).

34. Kim, J. et al. Rational understanding of substituent effects on multi carbazole thermally activated delayed fluorescence emitters. *J. Mater. Chem. C.* **10,** 7304-7310 (2022).

35. Hirata, S. Molecular physics of persistent room temperature phosphorescence and long-lived triplet excitons. *Appl. Phys. Rev.* **9,** 011304 (2022).

36. An, Z. F. et al. Stabilizing triplet excited states for ultralong organic phosphorescence. *Nat. Mater.* **14,** 685-690 (2015).

37. Ma, H. L. et al. Hydrogen Bonding-Induced Morphology Dependence of Long-Lived Organic Room-Temperature Phosphorescence: A Computational Study. *J. Phys. Chem. Lett.* **10,** 6948-6954 (2019).

38. Kim, D. H. et al. Efficient Photon Extraction in Top-Emission Organic Light-Emitting Devices Based on Ampicillin Microstructures. *Adv. Mater.* **34,** 2202866 (2022).

39. Li, C. et al. A Low-Cost Test Method for Accurate Detection of Different Excited-State Species with a Lifetime Span over 5 Orders of Magnitude in One Time Window. *Anal. Chem.* **95,** 8150-8155 (2023).

40. Chan, C. Y., Tanaka, M., Nakanotani, H. & Adachi, C. Efficient and stable sky-blue delayed fluorescence organic light-emitting diodes with CIE(y) below 0.4. *Nat. Commun.* **9,** 5036 (2018).

41. Fu, Y., Liu, H., Tang, B. Z. & Zhao, Z. J. Exploring Efficient Blue TADF Materials with Ultrafast Bipolar Charge Transport for High-Efficiency Thick-Layer OLEDs. *Adv. Funct. Mater.* **34,** 2401434 (2024).

42. Peng, X. L. et al. Purely Organic Room-Temperature Phosphorescence Molecule for High-Performance Non-Doped Organic Light-Emitting Diodes. *Angew. Chem., Int. Ed.* **63,** e202405418 (2024).

43. Sachnik, O. et al. Pure-blue single-layer organic light-emitting diodes based on trap-free hyperfluorescence. *Nat. Mater.* **24,** 1742-1748 (2025).

44. Kotadiya, N. B., Blom, P. W. M. & Wetzelaer, G.-J. A. H. Efficient and stable single-layer organic light-emitting diodes based on thermally activated delayed fluorescence. *Nat. Photon.* **13,** 765-769 (2019).

45. Li, Y. G. et al. Enhanced Operational Stability by Cavity Control of Single-Layer Organic Light-Emitting Diodes Based on Thermally Activated Delayed Fluorescence. *Adv. Mater.* **35,** 2304728 (2023).

46. Dahal, E. et al. Characterization of higher harmonic modes in Fabry-Perot microcavity organic light emitting diodes. *Sci. Rep.* **11,** 8456 (2021).

47. Chen, R. X., Liang, N. N. & Zhai, T. R. Dual-color emissive OLED with orthogonal polarization modes. *Nat. Commun.* **15,** 1331 (2024).

48. Miao, Y. Q. et al. Precise manipulation of the carrier recombination zone: a universal novel device structure for highly efficient monochrome and white phosphorescent organic light-emitting diodes with extremely small efficiency roll-off. *J. Mater. Chem. C.* **6,** 8122-8134 (2018).

49. Regnat, M., Pernstich, K. P., Zufle, S. & Ruhstaller, B. Analysis of the Bias-Dependent Split Emission Zone in Phosphorescent OLEDs. *ACS Appl. Mater. Interfaces.* **10,** 31552-31559 (2018).

50. Zhang, J. Y. et al. Highly Efficient and Robust Full-Color Organic Afterglow through 2D Superlattices Embedment. *Adv. Mater.* **34,** 2206712 (2022).

51. Peng, H. et al. On-demand modulating afterglow color of water-soluble polymers through phosphorescence FRET for multicolor security printing. *Sci. Adv.* **8,** eabk2925 (2022).

52. Jeon, W. S. et al. Ideal host and guest system in phosphorescent OLEDs. *Org. Electron.* **10,** 240-246 (2009).

53. Hua, J. et al. High-efficiency all-fluorescent white organic light-emitting diode based on TADF material as a sensitizer. *RSC Adv.* **13,** 31632-31640 (2023).

54. Meng, L.-C. & Hou, Y.-B. Electric-field modulated energy transfer in phosphorescent material-and fluorescent material-codoped polymer light-emitting diodes. *RSC Adv.* **14,** 12294-12302 (2024).

55. Vries, X. D., Coehoorn, R. & Bobbert, P. A. High energy acceptor states strongly enhance exciton transfer between metal organic phosphorescent dyes. *Nat. Commun.* **11,** 1292 (2020).

56. Yin, C. et al. Highly efficient and nearly roll-off-free electrofluorescent devices via multiple sensitizations. *Sci. Adv.* **8,** eabp9203 (2022).